

Observation of $B^\pm \rightarrow \omega K^\pm$ Decay

R.-S. Lu,²⁶ K. Abe,⁸ K. Abe,⁴¹ N. Abe,⁴⁴ R. Abe,²⁹ T. Abe,⁴² I. Adachi,⁸ H. Aihara,⁴³ Y. Asano,⁴⁸ T. Aso,⁴⁷ V. Aulchenko,² T. Aushev,¹² A. M. Bakich,³⁸ Y. Ban,³³ E. Banas,²⁷ I. Bedny,² P. K. Behera,⁴⁹ I. Bizjak,¹³ A. Bondar,² A. Bozek,²⁷ M. Bračko,^{20,13} T. E. Browder,⁷ B. C. K. Casey,⁷ M.-C. Chang,²⁶ P. Chang,²⁶ Y. Chao,²⁶ K.-F. Chen,²⁶ B. G. Cheon,³⁷ R. Chistov,¹² S.-K. Choi,⁶ Y. Choi,³⁷ Y. K. Choi,³⁷ M. Danilov,¹² L. Y. Dong,¹⁰ A. Drutskoy,¹² S. Eidelman,² V. Eiges,¹² C. W. Everton,²¹ C. Fukunaga,⁴⁵ N. Gabyshev,⁸ T. Gershon,⁸ B. Golob,^{19,13} A. Gordon,²¹ R. Guo,²⁴ J. Haba,⁸ T. Hara,³¹ Y. Harada,²⁹ H. Hayashii,²³ M. Hazumi,⁸ E. M. Heenan,²¹ T. Higuchi,⁴³ L. Hinz,¹⁸ T. Hokuue,²² Y. Hoshi,⁴¹ W.-S. Hou,²⁶ S.-C. Hsu,²⁶ H.-C. Huang,²⁶ T. Igaki,²² Y. Igarashi,⁸ T. Iijima,²² K. Inami,²² A. Ishikawa,²² R. Itoh,⁸ H. Iwasaki,⁸ Y. Iwasaki,⁸ H. K. Jang,³⁶ J. H. Kang,⁵² P. Kapusta,²⁷ S. U. Kataoka,²³ N. Katayama,⁸ H. Kawai,³ Y. Kawakami,²² N. Kawamura,¹ T. Kawasaki,²⁹ H. Kichimi,⁸ D. W. Kim,³⁷ Heejong Kim,⁵² H. J. Kim,⁵² H. O. Kim,³⁷ Hyunwoo Kim,¹⁵ S. K. Kim,³⁶ K. Kinoshita,⁵ P. Krokovny,² R. Kulasiri,⁵ S. Kumar,³² A. Kuzmin,² Y.-J. Kwon,⁵² G. Leder,¹¹ S. H. Lee,³⁶ J. Li,³⁵ D. Liventsev,¹² J. MacNaughton,¹¹ G. Majumder,³⁹ F. Mandl,¹¹ T. Matsuishi,²² S. Matsumoto,⁴ T. Matsumoto,⁴⁵ W. Mitaroff,¹¹ K. Miyabayashi,²³ Y. Miyabayashi,²² H. Miyake,³¹ H. Miyata,²⁹ G. R. Moloney,²¹ T. Mori,⁴ A. Murakami,³⁴ T. Nagamine,⁴² Y. Nagasaka,⁹ T. Nakadaira,⁴³ E. Nakano,³⁰ M. Nakao,⁸ J. W. Nam,³⁷ Z. Natkaniec,²⁷ K. Neichi,⁴¹ S. Nishida,¹⁶ O. Nitoh,⁴⁶ S. Noguchi,²³ T. Nozaki,⁸ S. Ogawa,⁴⁰ F. Ohno,⁴⁴ T. Ohshima,²² T. Okabe,²² S. Okuno,¹⁴ S. L. Olsen,⁷ W. Ostrowicz,²⁷ H. Ozaki,⁸ H. Palka,²⁷ C. W. Park,¹⁵ H. Park,¹⁷ L. S. Peak,³⁸ J.-P. Perroud,¹⁸ M. Peters,⁷ L. E. Pilonen,⁵⁰ N. Root,² K. Rybicki,²⁷ H. Sagawa,⁸ S. Saitoh,⁸ Y. Sakai,⁸ M. Satapathy,⁴⁹ A. Satpathy,^{8,5} O. Schneider,¹⁸ S. Schrenk,⁵ S. Semenov,¹² K. Senyo,²² R. Seuster,⁷ M. E. Sevir,²¹ H. Shibuya,⁴⁰ V. Sidorov,² J. B. Singh,³² N. Soni,³² S. Stanič,^{48,*} M. Starič,¹³ A. Sugi,²² A. Sugiyama,²² K. Sumisawa,⁸ T. Sumiyoshi,⁴⁵ K. Suzuki,⁸ S. Suzuki,⁵¹ T. Takahashi,³⁰ F. Takasaki,⁸ K. Tamai,⁸ N. Tamura,²⁹ J. Tanaka,⁴³ M. Tanaka,⁸ G. N. Taylor,²¹ Y. Teramoto,³⁰ S. Tokuda,²² M. Tomoto,⁸ T. Tomura,⁴³ S. N. Tovey,²¹ K. Trabelsi,⁷ T. Tsuboyama,⁸ T. Tsukamoto,⁸ S. Uehara,⁸ K. Ueno,²⁶ S. Uno,⁸ Y. Ushiroda,⁸ G. Varner,⁷ K. E. Varvell,³⁸ C. C. Wang,²⁶ C. H. Wang,²⁵ J. G. Wang,⁵⁰ M.-Z. Wang,²⁶ Y. Watanabe,⁴⁴ E. Won,¹⁵ B. D. Yabsley,⁵⁰ Y. Yamada,⁸ Y. Yamashita,²⁸ M. Yamauchi,⁸ P. Yeh,²⁶ Y. Yuan,¹⁰ J. Zhang,⁴⁸ Z. P. Zhang,³⁵ Y. Zheng,⁷ and D. Žontar⁴⁸

(The Belle Collaboration)

¹Aomori University, Aomori

²Budker Institute of Nuclear Physics, Novosibirsk

³Chiba University, Chiba

⁴Chuo University, Tokyo

⁵University of Cincinnati, Cincinnati OH

⁶Gyeongsang National University, Chinju

⁷University of Hawaii, Honolulu HI

⁸High Energy Accelerator Research Organization (KEK), Tsukuba

⁹Hiroshima Institute of Technology, Hiroshima

¹⁰Institute of High Energy Physics, Chinese Academy of Sciences, Beijing

¹¹Institute of High Energy Physics, Vienna

¹²Institute for Theoretical and Experimental Physics, Moscow

¹³J. Stefan Institute, Ljubljana

¹⁴Kanagawa University, Yokohama

¹⁵Korea University, Seoul

¹⁶Kyoto University, Kyoto

¹⁷Kyungpook National University, Taegu

¹⁸Institut de Physique des Hautes Énergies, Université de Lausanne, Lausanne

¹⁹University of Ljubljana, Ljubljana

²⁰University of Maribor, Maribor

²¹University of Melbourne, Victoria

²²Nagoya University, Nagoya

²³Nara Women's University, Nara

²⁴National Kaohsiung Normal University, Kaohsiung

²⁵National Lien-Ho Institute of Technology, Miao Li

²⁶National Taiwan University, Taipei

²⁷H. Niewodniczanski Institute of Nuclear Physics, Krakow

²⁸Nihon Dental College, Niigata

²⁹Niigata University, Niigata

- ³⁰Osaka City University, Osaka
³¹Osaka University, Osaka
³²Panjab University, Chandigarh
³³Peking University, Beijing
³⁴Saga University, Saga
³⁵University of Science and Technology of China, Hefei
³⁶Seoul National University, Seoul
³⁷Sungkyunkwan University, Suwon
³⁸University of Sydney, Sydney NSW
³⁹Tata Institute of Fundamental Research, Bombay
⁴⁰Toho University, Funabashi
⁴¹Tohoku Gakuin University, Tagajo
⁴²Tohoku University, Sendai
⁴³University of Tokyo, Tokyo
⁴⁴Tokyo Institute of Technology, Tokyo
⁴⁵Tokyo Metropolitan University, Tokyo
⁴⁶Tokyo University of Agriculture and Technology, Tokyo
⁴⁷Toyama National College of Maritime Technology, Toyama
⁴⁸University of Tsukuba, Tsukuba
⁴⁹Utkal University, Bhubaneswer
⁵⁰Virginia Polytechnic Institute and State University, Blacksburg VA
⁵¹Yokkaichi University, Yokkaichi
⁵²Yonsei University, Seoul
(Dated: October 29, 2018)

We report the first observation of the charmless two-body mode $B^\pm \rightarrow \omega K^\pm$ decay, and a new measurement of the branching fraction for the $B^\pm \rightarrow \omega \pi^\pm$ decay. The measured branching fractions are $\mathcal{B}(B^\pm \rightarrow \omega K^\pm) = (9.2_{-2.3}^{+2.6} \pm 1.0) \times 10^{-6}$ and $\mathcal{B}(B^\pm \rightarrow \omega \pi^\pm) = (4.2_{-1.8}^{+2.0} \pm 0.5) \times 10^{-6}$. We also measure the partial rate asymmetry of $B^\pm \rightarrow \omega K^\pm$ decays and obtain $A_{CP} = -0.21 \pm 0.28 \pm 0.03$. The results are based on a data sample of 29.4 fb^{-1} collected on the $\Upsilon(4S)$ resonance by the Belle detector at the KEKB e^+e^- collider.

PACS numbers: 13.25.Hw, 14.40.Nd

Charmless hadronic B decays are of interest not only for testing our current understanding of heavy quark physics, but also as modes to search for direct CP violation. The $B^- \rightarrow \omega \pi^-$ and ωK^- decays [1] are dominated by tree-level and gluonic penguin diagrams [2], respectively, illustrated in Fig. 1. Thus, their branching fractions can give us further insight into gluonic penguin diagrams, while interference between tree and penguin diagrams can lead to a measurable direct CP asymmetry.

In factorization models with $N_c \simeq 2-3$, where N_c is the effective number of colors, the $\omega \pi$ mode is larger than the ωK mode by a factor of 2 or more [2]. This result is borne out by further studies in the QCD factorization [3] and perturbative QCD (pQCD) [4] frameworks. In this letter, we report measurements of $B^- \rightarrow \omega K^-$ and $\omega \pi^-$ decays

that indicate that the former is more prominent, which may suggest the influence of nonfactorized effects.

The $B^- \rightarrow \omega K^-$ mode has an interesting history. It was first reported by CLEO in 1998 [5] with 3.9σ significance, but subsequently superseded by non-observation with a larger data set [6], a result that is supported by BABAR [7]. However, we report here a significant signal in this mode. The $B^- \rightarrow \omega \pi^-$ mode has been reported previously by the CLEO [6] and BABAR [7] collaborations at levels that are somewhat higher than our findings. The data used in this analysis were collected with the Belle detector [8] at KEKB [9], a double storage ring that collides 8 GeV electrons and 3.5 GeV positrons with a 22 mrad crossing angle. The data sample corresponds to an integrated luminosity of 29.4 fb^{-1} on the $\Upsilon(4S)$ resonance, containing 31.9 million $B\bar{B}$ pairs, and 2.3 fb^{-1} taken 60 MeV below the resonance.

Belle is a general-purpose detector with a 1.5 T superconducting solenoid magnet. Charged particle tracking, covering 86% of the total center-of-mass (CM) solid angle, is provided by a Silicon Vertex Detector (SVD) consisting of three concentric layers of double-sided silicon strip detectors, and a 50-layer Central Drift Chamber (CDC). Charged hadrons are distinguished by combining the responses from an array of Silica Aerogel Čerenkov Counters (ACC), a Time of Flight Counter sys-

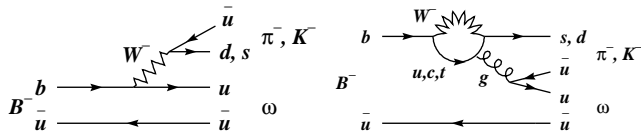


FIG. 1: Tree (left) and penguin (right) diagrams for $B^- \rightarrow \omega K^-$ and $B^- \rightarrow \omega \pi^-$ decays.

tem (TOF), and dE/dx measurements in the CDC. The combined response provides K/π separation of at least 2.5σ for laboratory momenta up to $3.5\text{ GeV}/c$. Photons and electrons are detected in an array of 8736 CsI(Tl) crystals (ECL) located inside the magnetic field and covering the entire solid angle of the charged particle tracking system. The 1.5 T magnetic field is returned via a flux return that consists of 4.7 cm thick steel plates interspersed with resistive plate chambers to detect muons and K_L mesons (KLM). The Belle detector is described in detail elsewhere [8].

Well reconstructed tracks that are inconsistent with being electrons or muons are identified as kaon or pions according to a K/π likelihood ratio (KID), $\mathcal{L}_K/(\mathcal{L}_\pi + \mathcal{L}_K)$, where the $\mathcal{L}_{K(\pi)}$ are likelihoods derived from the responses of the dE/dx , ACC and TOF systems. Candidate π^0 mesons are reconstructed from pairs of photons, each consisting of energy clusters greater than 50 MeV in the ECL, with $m_{\gamma\gamma}$ inside a $\pm 3\sigma$ ($\sigma = 5.4\text{ MeV}/c^2$) mass window around the π^0 mass [10]. A mass-constrained fit is then performed to improve the π^0 momentum resolution. Candidate ω mesons are formed from $\pi^+\pi^-\pi^0$ combinations with an invariant mass that is within $\pm 30\text{ MeV}/c^2$ of the nominal ω mass [10]. (The natural width of the ω meson is 8.9 MeV.) To further reduce the large combinatorial background from low energy photons and π^0 s, an ω candidate is discarded if the daughter π^0 s CM momenta is below $350\text{ MeV}/c$. This selection on π^0 CM momentum loses 16% of the signal, but removes 60% of the combinatorial background.

We combine an ω candidate with either a K^- or a π^- track to form a B^- candidate. As part of this procedure, the momenta of the three charged tracks are recalculated subject to the constraint that they originate from the interaction point. Using the CM beam energy $E_{\text{beam}}^{\text{CM}} = \sqrt{s}/2 = 5.29\text{ GeV}$ and the measured CM energy E_B^{CM} and momentum p_B^{CM} of the B candidate, we form two kinematic variables to select the signal events: the beam-constrained mass $M_{bc} = \sqrt{(E_{\text{beam}}^{\text{CM}})^2 - (p_B^{\text{CM}})^2}$ and the energy difference $\Delta E = E_B^{\text{CM}} - E_{\text{beam}}^{\text{CM}}$.

The major background for this analysis is from continuum $e^+e^- \rightarrow q\bar{q}$ production, where q is a light quark (u , d , s , or c). The jet-like continuum events are suppressed relative to the more spherical $B\bar{B}$ events by characterization of the event shape, which is implemented with a Fisher discriminant [11] containing six modified Fox-Wolfram moments [12, 13]. There are two types of combinatorial backgrounds from continuum events: fake ω mesons and fake B mesons. The former is suppressed using the cross product $|\vec{P}_+ \times \vec{P}_-|$ of the momenta of the charged pion daughters in the ω meson rest frame. The latter is suppressed using the B candidate flight direction relative to the positron beam axis, and the helicity angle of the candidate ω meson relative to the B meson. The helicity angle, θ_{hel} , is defined as the angle between

the B flight direction and the vector perpendicular to the ω decay plane in the ω rest frame. We use a likelihood ratio technique that combines the Fisher discriminant, the cross product of the momenta of the charged pions from the ω , the B flight direction, and the cosine of the helicity angle, $\cos\theta_{\text{hel}}$, to suppress the continuum background relative to the $B \rightarrow \omega h$ ($h = \pi$ or K) signal. The probability density functions (PDFs) for signal and background are constructed using Monte-Carlo (MC) events. The background PDFs are in good agreement with those determined from on-resonant sideband data ($M_{bc} < 5.26\text{ GeV}/c^2$ and $|\Delta E| < 0.3\text{ GeV}$). With these PDFs, we determine signal (\mathcal{L}_S) and background (\mathcal{L}_{BG}) likelihoods for each event that are used to form the normalized likelihood ratio $\mathcal{R} = \mathcal{L}_S/(\mathcal{L}_S + \mathcal{L}_{\text{BG}})$; we discard events with $\mathcal{R} < 0.85$. This selection retains 50% of the signal while rejecting 95% of the continuum background.

To study background from B decays through the $b \rightarrow c$ transition and charmless B decays such as $B \rightarrow \omega K^*$ and $B \rightarrow \omega\rho$, and non-resonant $B \rightarrow K^-\pi^+\pi^-\pi^0$ decays, we used MC samples up to 20 times larger than our data sample, assuming the best known branching fraction for each decay [14]. We find negligible backgrounds from these decays in the $M_{bc}-\Delta E$ signal region ($M_{bc} > 5.27\text{ GeV}/c^2$ and $|\Delta E| < 0.1\text{ GeV}$).

The signal is extracted using M_{bc} and ΔE as independent variables in an unbinned maximum likelihood fit for events with $|\Delta E| < 0.3\text{ GeV}$ and $M_{bc} > 5.2\text{ GeV}/c^2$. The signal PDF for M_{bc} is a Gaussian and that for ΔE is the parameterization of Ref. [15]. The parameters are determined from MC simulation and calibrated by the decay chain $B^- \rightarrow D^0\pi^-$, $D^0 \rightarrow K^-\pi^+\pi^0$. The resolutions determined from MC are $3\text{ MeV}/c^2$ for M_{bc} and 24 MeV for ΔE . The PDF of continuum background for M_{bc} is an empirically determined threshold function [16] that is obtained from the sideband data ($\Delta E > 0.1\text{ GeV}$), while the PDF for ΔE is a linear polynomial obtained from the data ($M_{bc} > 5.27\text{ GeV}/c^2$) before the \mathcal{R} cut. PDFs for other background sources are included: charmless B decays that survive the selection criteria and signal events with charged kaons misidentified as pions or vice versa. (In the last case, the PDFs have the same shape as signal except that the central value of ΔE is shifted by 45 MeV.)

The signal yields from the maximum likelihood fit are summarized in Table I. The M_{bc} and ΔE distributions of candidate events and the best fit curves are shown in Fig. 2. The signal yields are $18.9_{-4.7}^{+5.4}$ and $10.4_{-4.3}^{+4.7}$ events for the ωK^- and $\omega\pi^-$ modes, respectively. The expected reflection due to π - K misidentification is 0.7 ± 0.3 (2.0 ± 0.6) events for the ωK^- ($\omega\pi^-$) mode; the fit gives 0.0 ± 2.4 (0.0 ± 3.9) events.

The statistical significance quoted in Table I is defined as $\sqrt{-2\ln(\mathcal{L}(0)/\mathcal{L}_{\text{max}})}$ where \mathcal{L}_{max} is the maximized likelihood at the nominal signal yield and $\mathcal{L}(0)$ is the likelihood with the signal yield fixed at zero. We observe

TABLE I: The signal yields, statistical significances (Σ), efficiencies (ϵ), branching fractions (\mathcal{B}), and the 90% confidence level upper limit (UL) of the branching fraction for the $\omega\pi^-$ mode are listed. The efficiencies include the ω decay branching fraction.

	Signal yield	Σ	ϵ (%)	\mathcal{B} ($\times 10^{-6}$)	UL ($\times 10^{-6}$)
ωK^-	$18.9_{-4.7}^{+5.4} \pm 0.6$	6.0σ	6.0	$9.2_{-2.3}^{+2.6} \pm 1.0$	-
$\omega\pi^-$	$10.4_{-4.3}^{+4.7+0.4} \pm 0.6$	3.3σ	7.7	$4.2_{-1.8}^{+2.0} \pm 0.5$	8.1

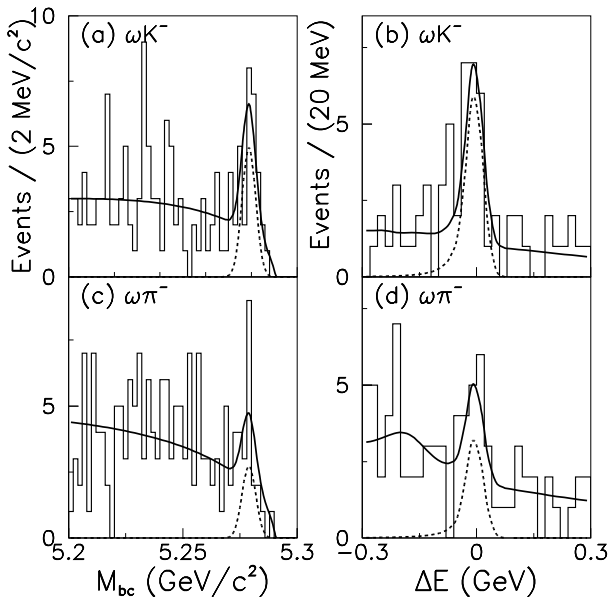


FIG. 2: The M_{bc} (left) and ΔE (right) distributions of the candidate events (histograms), the best fits (solid curves) and signal components (dashed curves).

18.9 signal events for $B^- \rightarrow \omega K^-$ with 6.0σ significance and find 10.4 $\omega\pi^-$ events with 3.3σ significance. Since the latter has less than 4σ significance, we use the 90% confidence level upper limit (N_S^{UL}) of 17.3 events on $B^- \rightarrow \omega\pi^-$ yield, determined by integrating the likelihood as a function of the number of signal events to 90% of its total area.

We study the systematic error associated with the fit by varying the parameters in the fitting functions by 1σ from their nominal values. The change in the signal yield from each variation is added in quadrature to obtain an overall systematic error associated with the fit. The systematic errors in the detection efficiencies of the ω meson and the high-momentum K^- and π^- mesons are 8.5% and 2.2%, respectively, which are determined from detailed studies of charged particle tracking, π^0 detection, and particle identification. A 5% systematic uncertainty

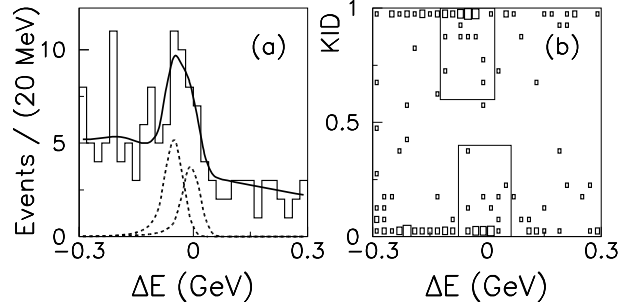


FIG. 3: The (a) ΔE distribution and (b) scatter plot of KID likelihood ratio versus ΔE for the ωh^- mode. The solid curve shows the fit result with the signal components shown by dashed curves.

is assigned to the continuum suppression cut, which is obtained by applying a similar procedure to data and MC samples of $B^- \rightarrow D^{*0}\pi^-$ events. The combined uncertainty of the efficiency is 10.1%.

The branching fractions in Table I are calculated assuming equal numbers of B^+B^- and $B^0\bar{B}^0$ pairs in our data sample. The uncertainty in the number of $B\bar{B}$ events, 1%, is taken into account and included in the systematic error for the branching fraction. The upper limit of the branching fraction of $\omega\pi^-$ decay is calculated after increasing N_S^{UL} and reducing the efficiency by their respective systematic error.

Our branching fraction result for $B^- \rightarrow \omega K^-$ is larger than that for $B^- \rightarrow \omega\pi^-$. As a consistency check, we also performed the analysis without KID information. Figure 3 shows the ΔE distribution and a scatter plot of the KID likelihood ratio versus ΔE for the ωh^- candidates. In these plots, we use the π^- mass for the high momentum hadron track. This causes a -45 MeV difference between the peak positions of ωK^- and $\omega\pi^-$ signals. The ΔE distribution is fitted with ωK^- and $\omega\pi^-$ signals, continuum background, and charmless background components. The signal yields are 17.1 ± 7.7 and 12.1 ± 7.0 events for ωK^- and $\omega\pi^-$, respectively, and are consistent with the results using the KID for K/π separation. The scatter plot in Fig. 3(b) shows the distribution of events in KID versus ΔE . The large rectangles, which cover the $\pm 3\sigma$ signal regions in ΔE and high or low kaon probability, contain enhancements at the appropriate places for both modes.

We also examine the properties of the ω candidates to confirm the $B^- \rightarrow \omega K^-$ signal. The $B^- \rightarrow \omega K^-$ signal yield in $\pi^+\pi^-\pi^0$ invariant mass bins is shown in Fig. 4(a). A clear signal at the ω mass is seen. The fitted number of ω mesons is 18.0 ± 5.0 which is consistent with the ωK^- signal yield. Figure 4(b) shows the $B^- \rightarrow \omega K^-$ signal yield in $\cos\theta_{hel}$ bins. The requirement on

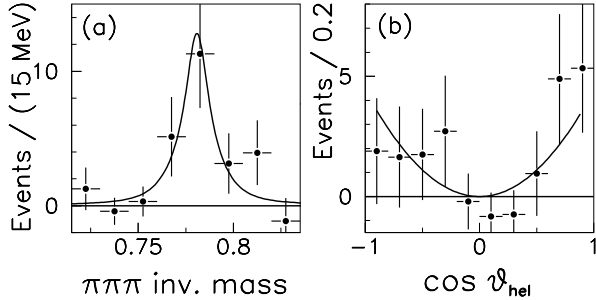


FIG. 4: The $B^- \rightarrow \omega K^-$ signal yield in bins of (a) $\pi^+\pi^-\pi^0$ invariant mass and (b) cosine of the ω helicity angle. The solid curve shows the fit result.

the likelihood ratio has been applied without including the helicity angle variable. The distribution is consistent with the expected $\cos^2 \theta_{\text{hel}}$ distribution.

We also measure the partial rate asymmetry in $B^\pm \rightarrow \omega K^\pm$ decays to search for direct CP violation. The asymmetry is defined as

$$\mathcal{A}_{CP} = \frac{N(\omega K^-) - N(\omega K^+)}{N(\omega K^-) + N(\omega K^+)}.$$

An application of the same event extraction and fitting procedure to the B^- and B^+ candidates separately yields 7.3 ± 3.5 and 11.2 ± 3.7 events for ωK^- and ωK^+ , respectively, and an asymmetry value $\mathcal{A}_{CP} = -0.21 \pm 0.28 \pm 0.03$. The systematic error includes the uncertainty associated with the fit procedure as well as a contribution of 1% due to detector bias in reconstruction of positive and negative high-momentum kaon tracks. The 90% confidence level interval $-0.70 < \mathcal{A}_{CP} < 0.28$ is obtained by assuming a Gaussian statistical error convolved with the systematic error.

Our combined branching fraction of $(13.4^{+3.3}_{-2.9} \pm 1.1) \times 10^{-6}$ for $B^- \rightarrow \omega h^-$ ($h = \pi$ or K) agrees with CLEO's number, $(14.3^{+3.6}_{-3.2} \pm 2.0) \times 10^{-6}$ [6], although the individual branching fractions are not totally consistent. Our large $B^- \rightarrow \omega K^-$ branching fraction also disagrees with the upper limit of 4×10^{-6} reported by the BABAR collaboration [7], although our $B^- \rightarrow \omega \pi^-$ result is not in conflict. We note that BABAR's combined branching fraction for $B^- \rightarrow \omega h^-$ ($h = \pi$ or K) is low compared to CLEO and our result.

The large $B^- \rightarrow \omega K^-$ branching fraction and relatively low $B^- \rightarrow \omega \pi^-$ rate cannot be easily accounted for either by generalized factorization [2] with $N_c \simeq 2-3$ or by calculations based on pQCD [3, 4]. To accommodate the large $B^- \rightarrow \omega K^-$ branching fraction that we observe, it appears that N_c has to deviate significantly from 3 [17], indicating the presence of large non-factorizable effects.

In summary, using 31.9 million $B\bar{B}$ pairs collected

with the Belle detector, we report the first observation of the $B^- \rightarrow \omega K^-$ decay with branching fraction $\mathcal{B}(B^- \rightarrow \omega K^-) = (9.2^{+2.6}_{-2.3} \pm 1.0) \times 10^{-6}$; the statistical significance of the above signal is 6.0σ . We also measure $\mathcal{B}(B^- \rightarrow \omega \pi^-) = (4.2^{+2.0}_{-1.8} \pm 0.5) \times 10^{-6}$, with a statistical significance of 3.3σ . The partial rate asymmetry for $B^\pm \rightarrow \omega K^\pm$ decays is found to be $\mathcal{A}_{CP} = -0.21 \pm 0.28 \pm 0.03$, corresponding to a 90% confidence level interval of $-0.70 < \mathcal{A}_{CP} < 0.28$.

We wish to thank the KEKB accelerator group for the excellent operation of the KEKB accelerator. We acknowledge support from the Ministry of Education, Culture, Sports, Science, and Technology of Japan and the Japan Society for the Promotion of Science; the Australian Research Council and the Australian Department of Industry, Science and Resources; the National Science Foundation of China under contract No. 10175071; the Department of Science and Technology of India; the BK21 program of the Ministry of Education of Korea and the CHEP SRC program of the Korea Science and Engineering Foundation; the Polish State Committee for Scientific Research under contract No. 2P03B 17017; the Ministry of Science and Technology of the Russian Federation; the Ministry of Education, Science and Sport of the Republic of Slovenia; the National Science Council and the Ministry of Education of Taiwan; and the U.S. Department of Energy.

* on leave from Nova Gorica Polytechnic, Nova Gorica

- [1] Charge conjugate modes are implicitly included throughout the paper.
- [2] A. Ali, G. Kramer and C. D. Lu, Phys. Rev. D **58**, 094009 (1998); Y. H. Chen, H. Y. Cheng, B. Tseng and K. C. Yang, Phys. Rev. **D60**, 094014 (1999).
- [3] D. S. Du, H. J. Gong, J. F. Sun, D. S. Yang and G. H. Zhu, Phys. Rev. D **65**, 094025 (2002).
- [4] C. D. Lu and M. Z. Yang, Eur. Phys. J. C **23**, 275 (2002); C. H. Chen, Phys. Lett. B **525**, 56 (2002).
- [5] CLEO Collaboration, T. Bergfeld *et al.*, Phys. Rev. Lett. **81**, 272 (1998).
- [6] CLEO Collaboration, C.P. Jessop *et al.*, Phys. Rev. Lett. **85**, 2881 (2000).
- [7] BABAR collaboration, B. Aubert *et al.*, Phys. Rev. Lett. **87**, 221802 (2001).
- [8] Belle Collaboration, A. Abashian *et al.*, Nucl. Instrum. and Meth. **A479**, 117 (2002).
- [9] E. Kikutani ed., KEK Preprint 2001-157 (2001), to appear in Nucl. Instrum. and Meth. **A**.
- [10] Particle Data Group, D. E. Groom *et al.*, Eur. Phys. J. C **15**, 1 (2000).
- [11] R. A. Fisher, Annals of Eugenics **7**, 179 (1936).
- [12] Belle Collaboration, K. Abe *et al.*, Phys. Rev. Lett. **87**, 101801 (2001).
- [13] G. C. Fox and S. Wolfram, Phys. Rev. Lett. **41**, 1581 (1978).
- [14] CLEO Collaboration, M. Bishai *et al.*, arXiv:hep-ex/9908018.

- [15] Crystal Ball Collaboration, J. E. Gaiser *et al.*, Phys. Rev. **D34**, 711 (1986).
- [16] ARGUS Collaboration, H. Albrecht *et al.*, Phys. Lett. **B241**, 278 (1990).
- [17] N. G. Deshpande, B. Dutta and S. Oh, Phys. Lett. B **473**, 141 (2000); G. Kramer, W. F. Palmer and H. Simma, Z. Phys. C **66**, 429 (1995).